

Electronic Supplementary Material (ESI)

Supporting Information

A microporous metal-organic framework with commensurate adsorption and highly selective separation of xenon

Shunshun Xiong^a, Youjin Gong^a, Shuanglin Hu^a, Xiaonan Wu^a, Wei Li^a, Yabing He^c, Banglin Chen^{b*} and Xiaolin Wang^{a*}

- a. Institute of Nuclear Physics and Chemistry, China Academy of Engineering Physics, Mianyang, Sichuan, 621900, P. R. China. E-mail: xlwang@caep.cn.
- b. Department of Chemistry, University of Texas at San Antonio, One UTSA Circle, San Antonio, Texas 78249-0698, United States. E-mail: banglin.chen@utsa.edu.
- c. Key Laboratory of the Ministry of Education for Advanced Catalysis Materials, Institute of Physical Chemistry, Zhejiang Normal University, Jinhua 321004, China.

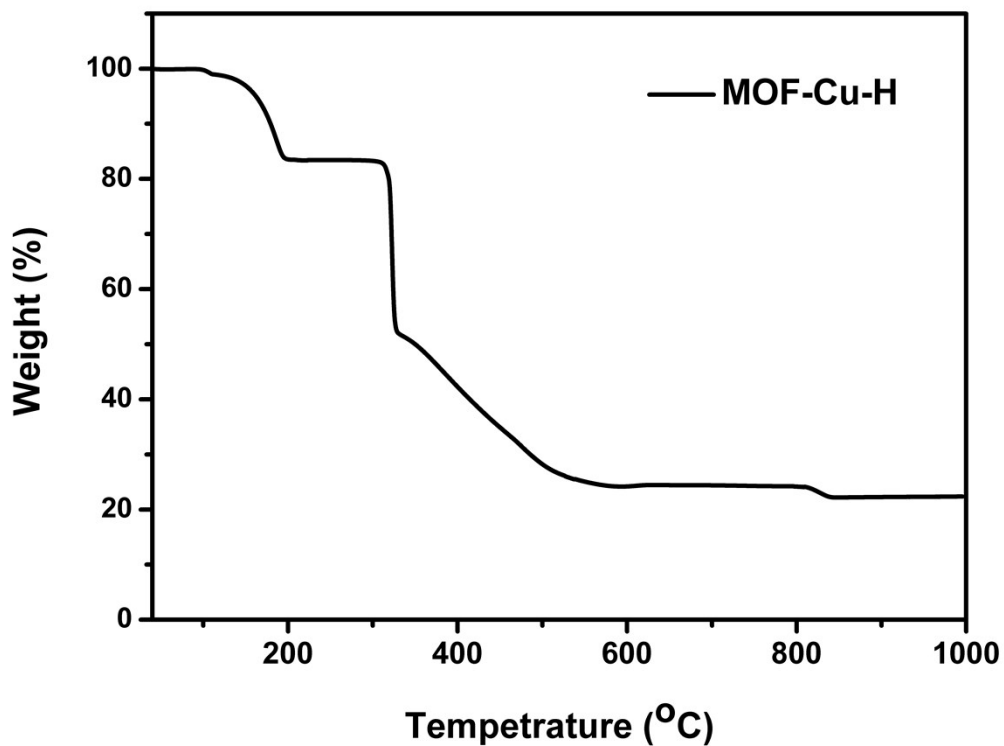


Figure S1. TGA curves of as-synthesized MOF-Cu-H.

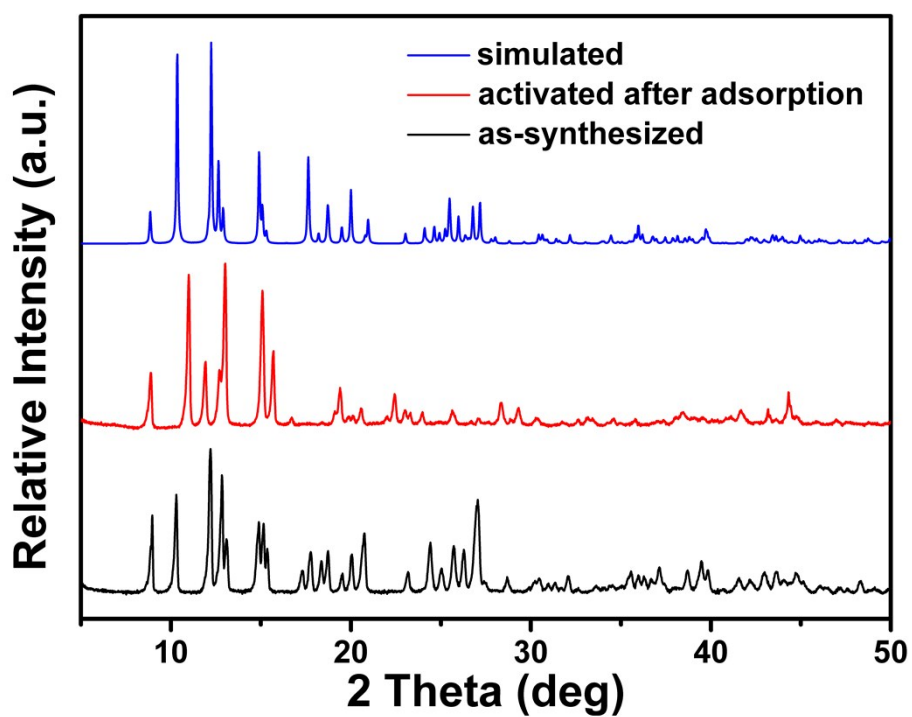


Figure S2. PXRD patterns of MOF-Cu-H samples.

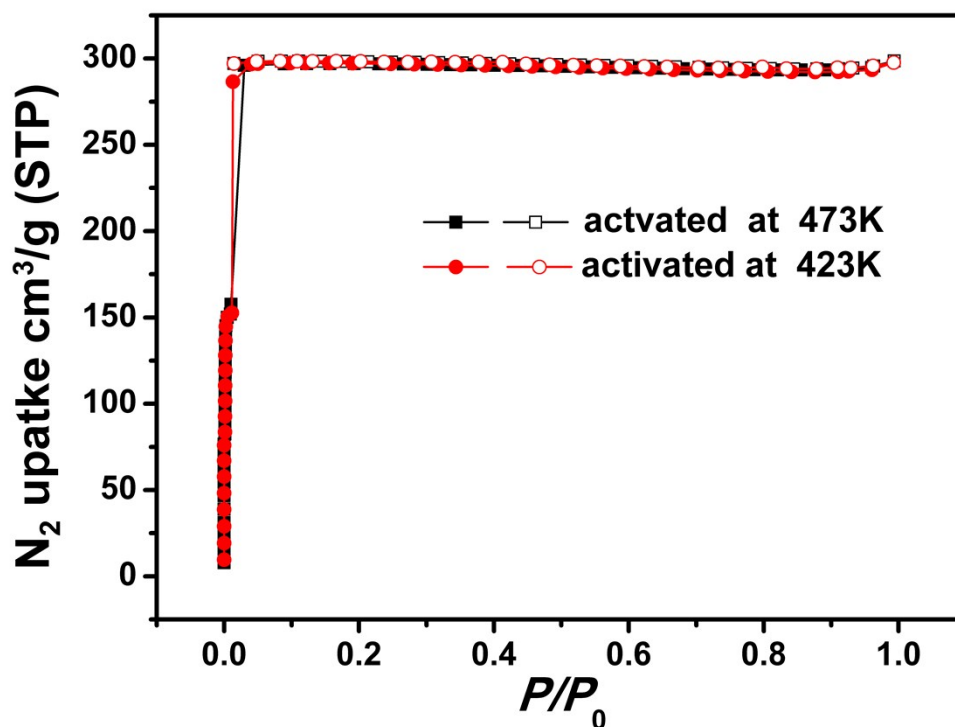


Figure S3. N₂ adsorption (closed) / desorption (open) isotherms for activated MOF-Cu-H samples at 77K. Samples activated at 473K (black), samples activated at 423K (red). The Langmuir (Brunauer-Emmet-Teller, BET) surface areas are calculated to be 1259.5 (874.8) m²/g for MOF-Cu-H samples activated at 473K.

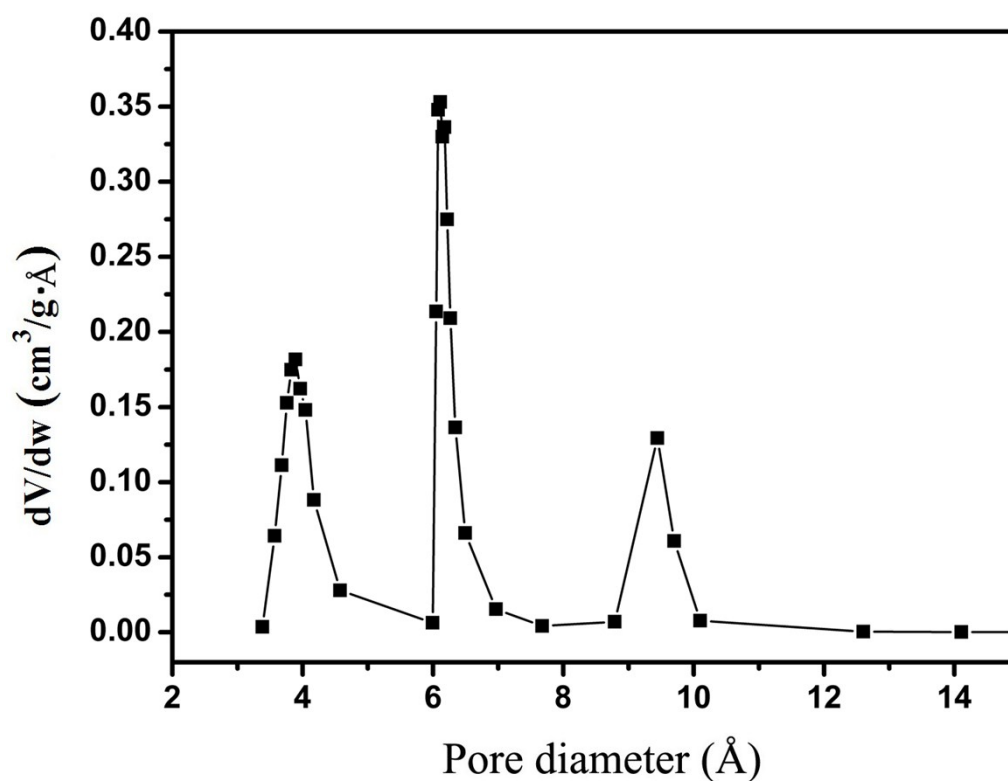


Figure S4. Pore size distribution for MOF-Cu-H samples activated at 423K using Horvath-Kawazoe (HK) model.

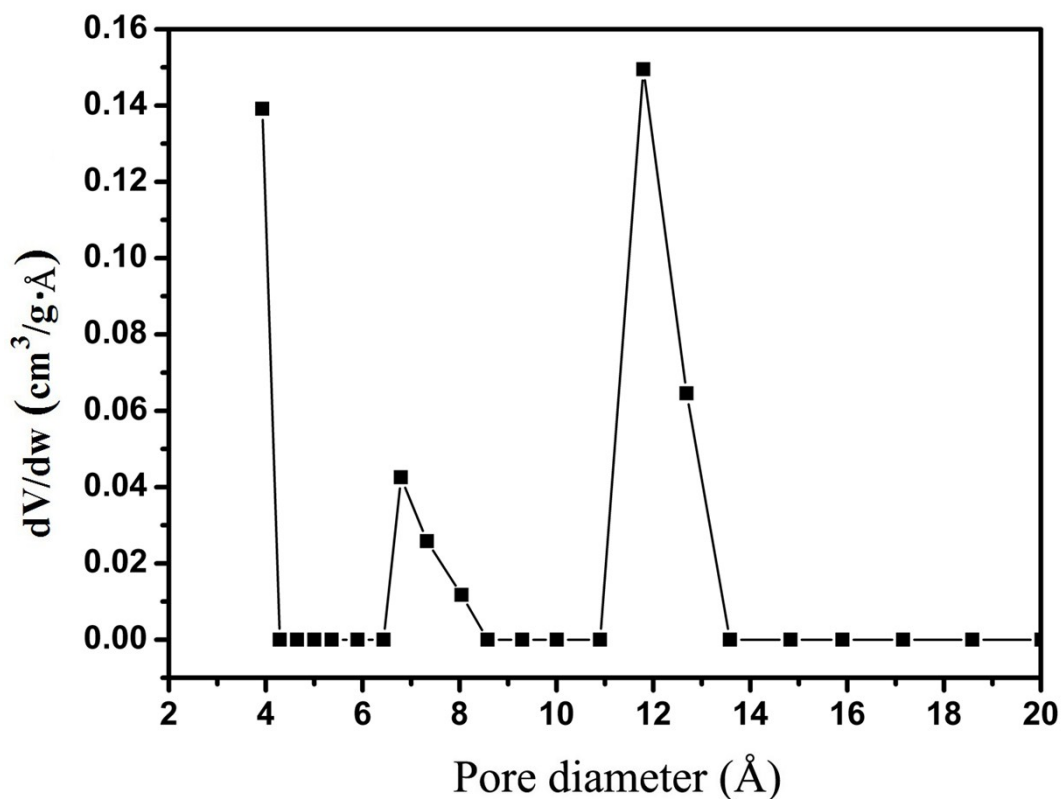


Figure S5. Pore size distribution for MOF-Cu-H samples activated at 423K using Non Local Density Functional Theory (NLDFT) model.

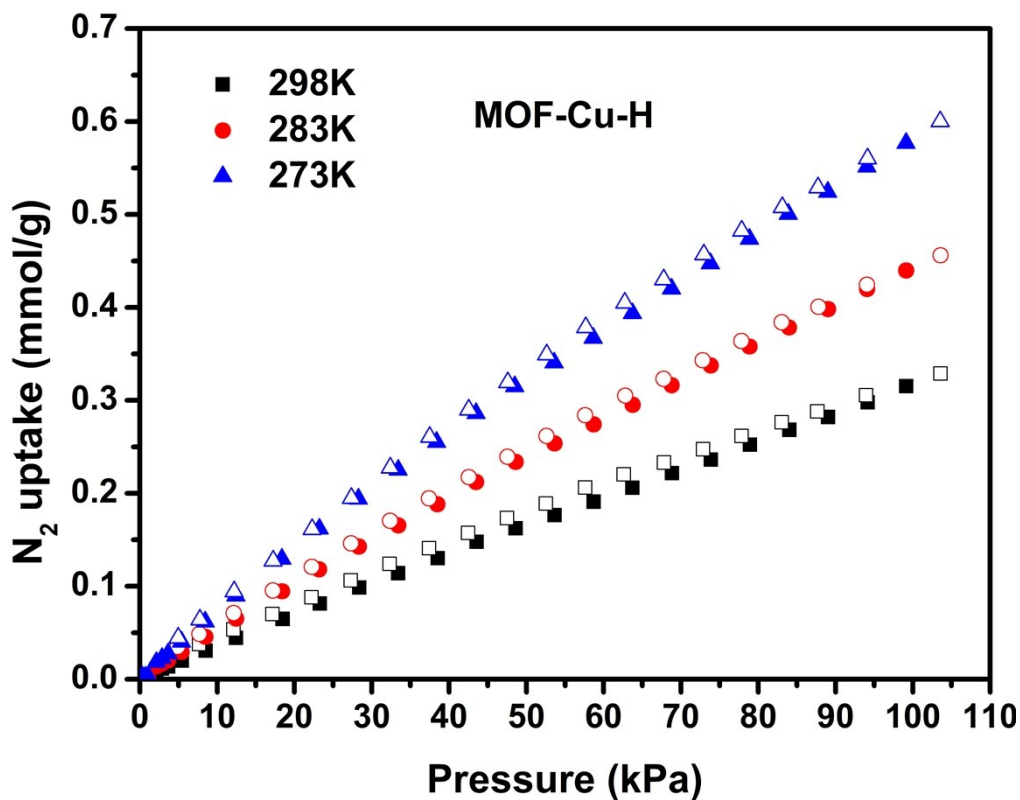


Figure S6. N₂ adsorption isotherms for MOF-Cu-H, at different temperatures (298K, 283K and 273K).

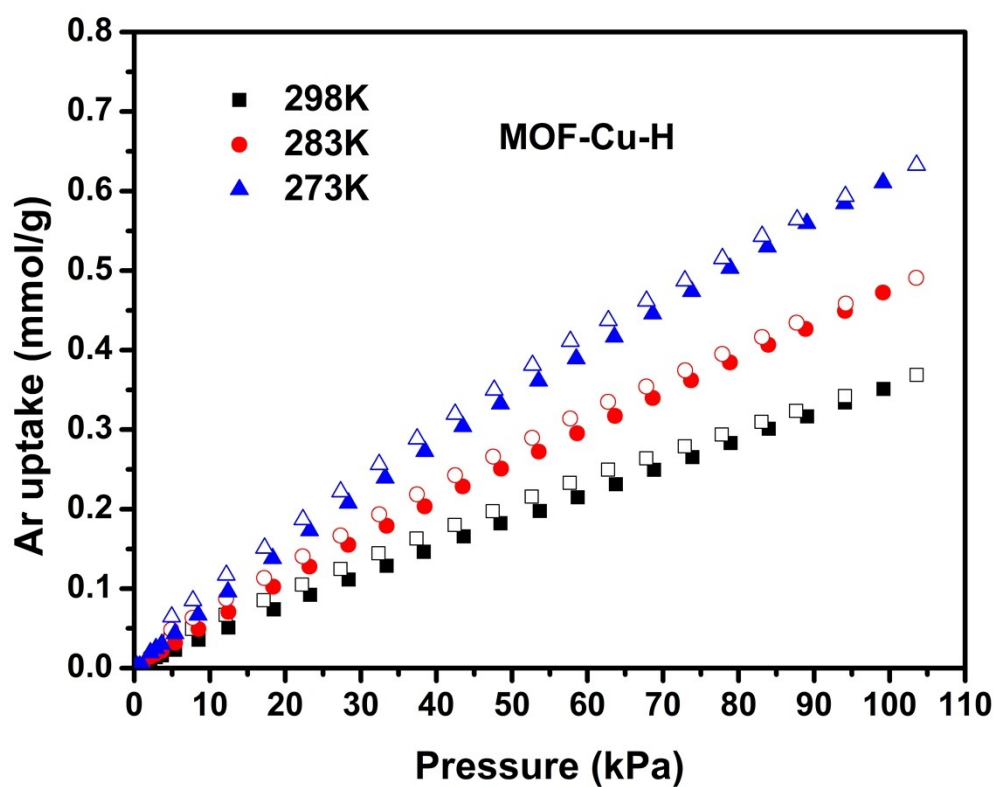


Figure S7. Ar adsorption isotherms for MOF-Cu-H, at different temperatures (298K, 283K and 273K).

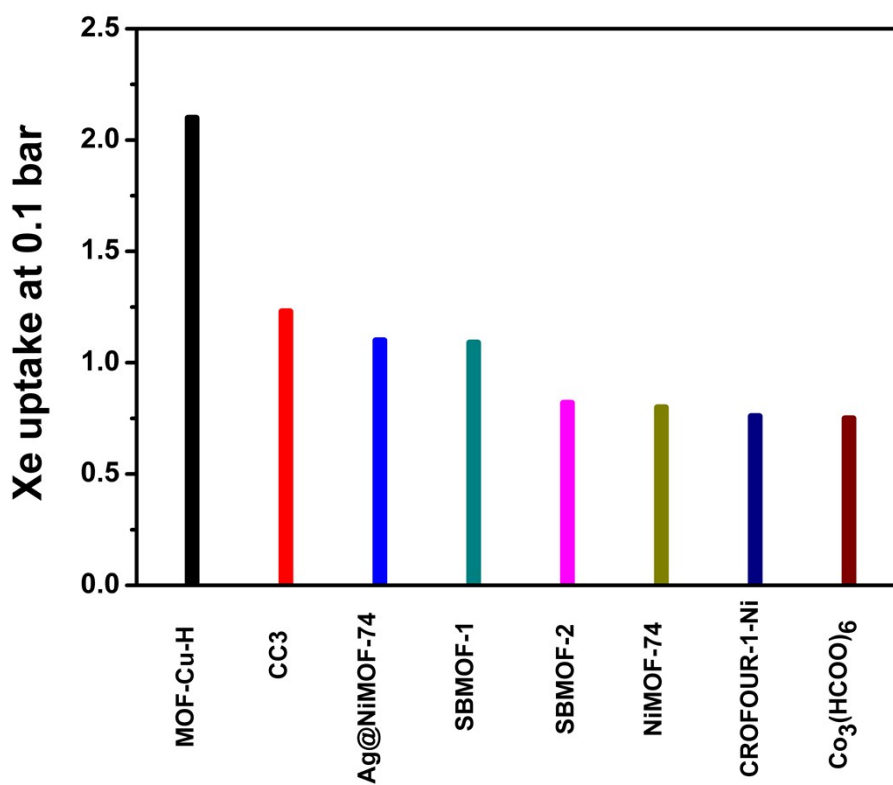


Figure S8. Bar plots showing Xe uptakes of selected porous materials at 298K and 0.1 bar

Adsorption kinetics experiments

Adsorption kinetic measurements of pure gases were performed using a Rubotherm gravimetric–densimetric apparatus (Bochum, Germany) (Supplementary Fig. 13), composed mainly of a magnetic suspension balance and a network of valves, mass flowmeters and temperature and pressure sensors. The magnetic suspension balance overcomes the disadvantages of other commercially available gravimetric instruments by separating the sensitive microbalance from the sample and the measuring atmosphere and is able to perform adsorption measurements across a wide pressure range, that is, from 0 to 5MPa. The adsorption temperature may also be controlled within the range of 77 to 423K. In a typical adsorption experiment, the adsorbent is precisely weighed and placed in a basket suspended by a permanent magnet through an electromagnet. The cell in which the basket is housed is then closed and vacuum or high pressure is applied. The gravimetric method allows the direct measurement of the reduced gas adsorbed amount Ω . Correction for the buoyancy effect is required to determine the excess and absolute adsorbed amount using equations 3 and 4, where $V_{\text{adsorbent}}$ and V_{ss} and $V_{\text{adsorbed phase}}$ refer to the volume of the adsorbent, the volume of the suspension system and the volume of the adsorbed phase, respectively.

$$\Omega = m_{\text{absolute}} - \rho_{\text{gas}} (V_{\text{adsorbent}} + V_{\text{ss}} + V_{\text{adsorbed-phase}}) \quad (1)$$

$$\Omega = m_{\text{excess}} - \rho_{\text{gas}} (V_{\text{adsorbent}} + V_{\text{ss}}) \quad (2)$$

The buoyancy effect resulted from the adsorbed phase maybe taken into account via correlation with the pore volume or with the theoretical density of the sample.

Kinetic studies of Xe and Kr adsorption on MOF-Cu-H, MOF-Cu-Me and MOF-Cu-F was carried out using the Rubotherm gravimetric apparatus operating in dynamic regime. Initially, crystal samples was properly evacuated at 403K in vacuum. In order to achieve an immediate constancy of pressure (0.5bar) during kinetics tests and avoid the often noisy uptake during the rapid introduction of the studied gas, an initial baseline was set-up using helium gas at 0.5 bar, then the studied single gas (Xe or Kr) is flushed with a flow of 100 ml/min to avoid any dependence of the kinetics on the mass flow controller.

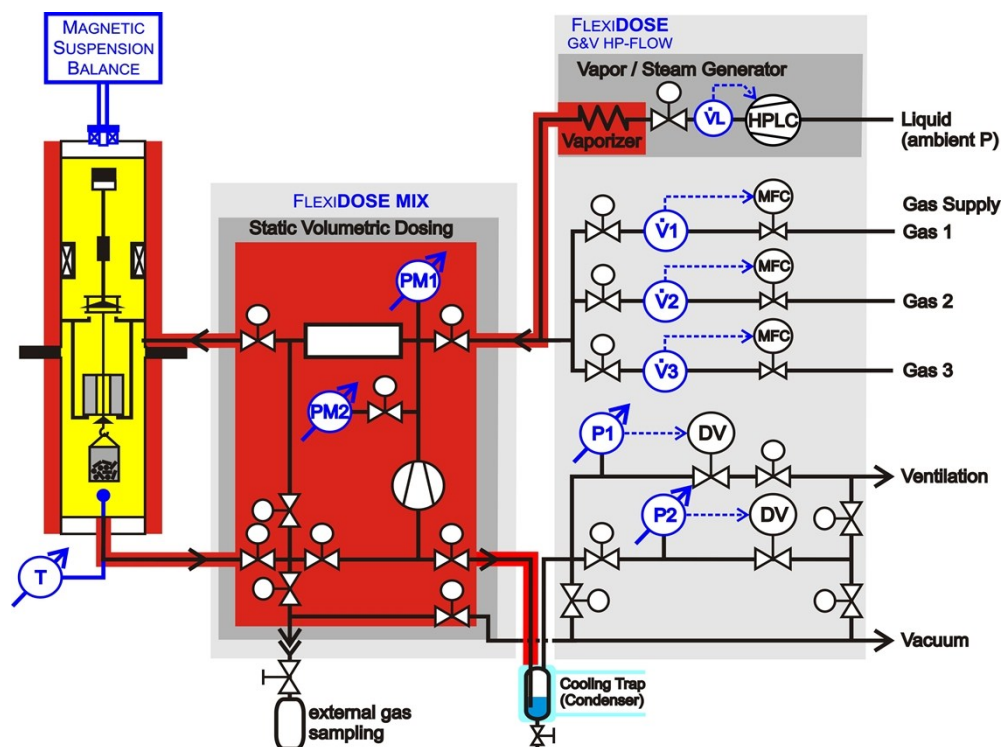


Figure S9. Representation of the Rubotherm gravimetric-densimetric-gas analysis (GDGA) apparatus for adsorption kinetics experiments

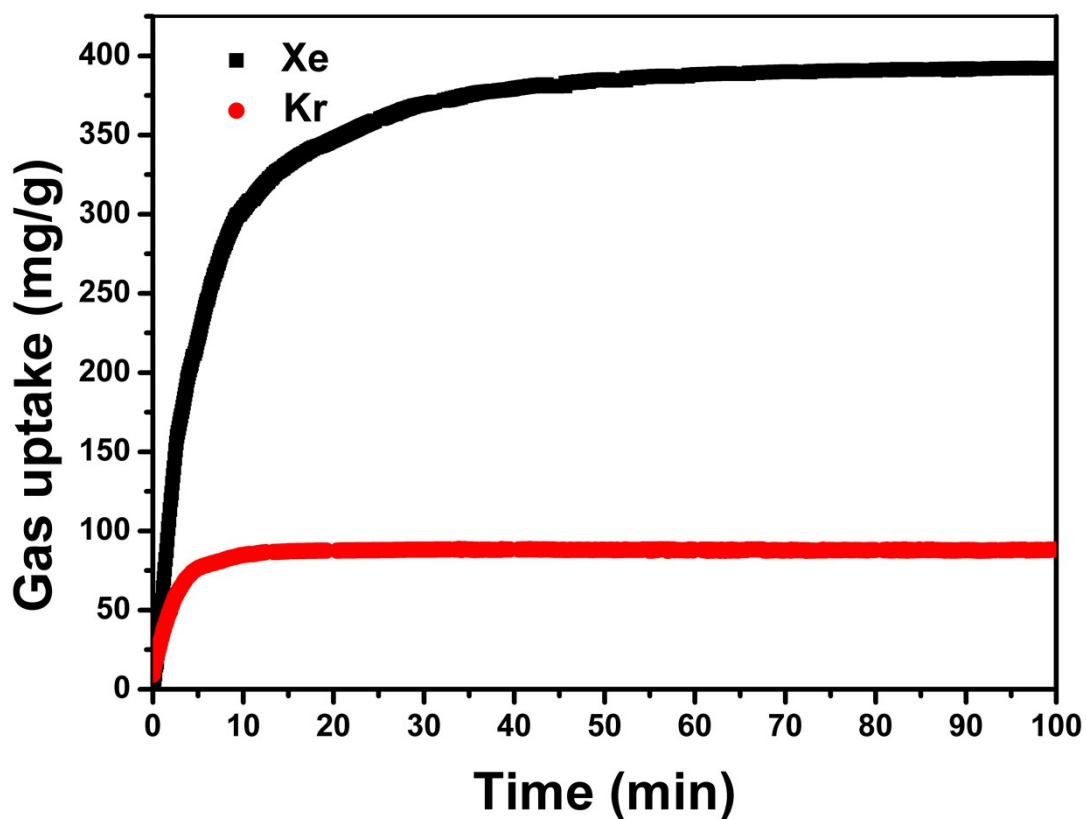


Figure S10. Kinetics of adsorption of MOF-Cu-H for single gas (Xe or Kr) at 298 K and 0.5 bar.

Powder X-ray diffraction Patterns

Powder X-ray diffraction (PXRD) patterns were recorded by a Bruker D8-advanture Powder X-ray Diffractometer Instrument operated at 40 kv and 44 mA with a scan of 1.0 deg min^{-1} . The activated samples of MOF-Cu-H were put into the system with Nitrogen atmosphere protection. The samples were heated with $10^\circ\text{C}/\text{min}$ and maintained at testing temperature for 10 minutes for equilibration.

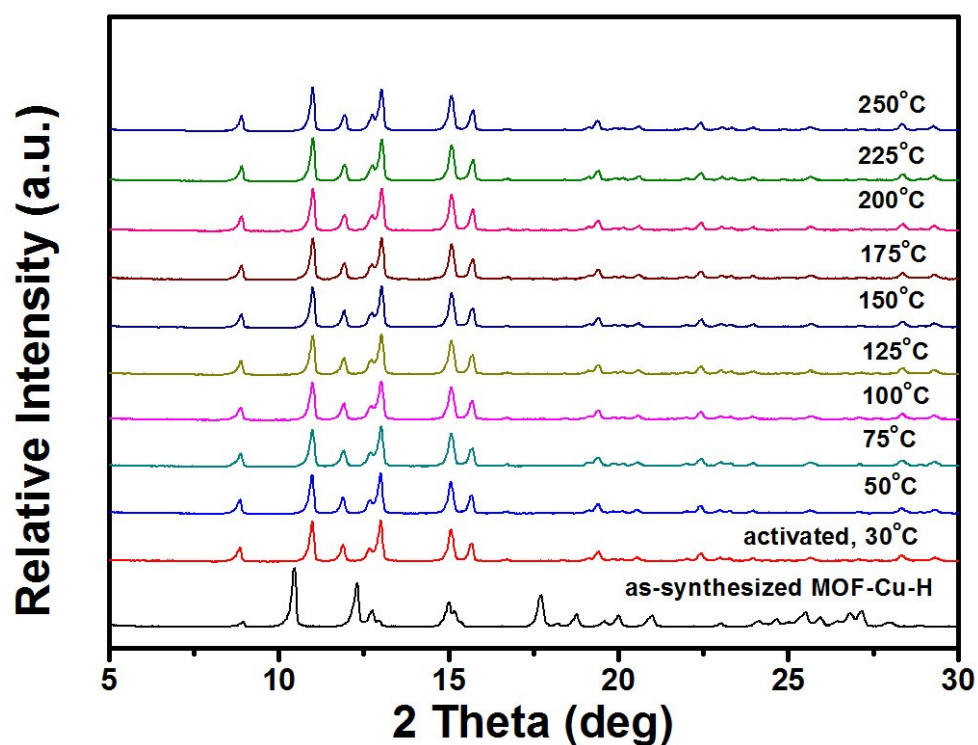


Figure S11. Temperature-variant Powder X-ray diffraction (PXRD) patterns for MOF-Cu-H.

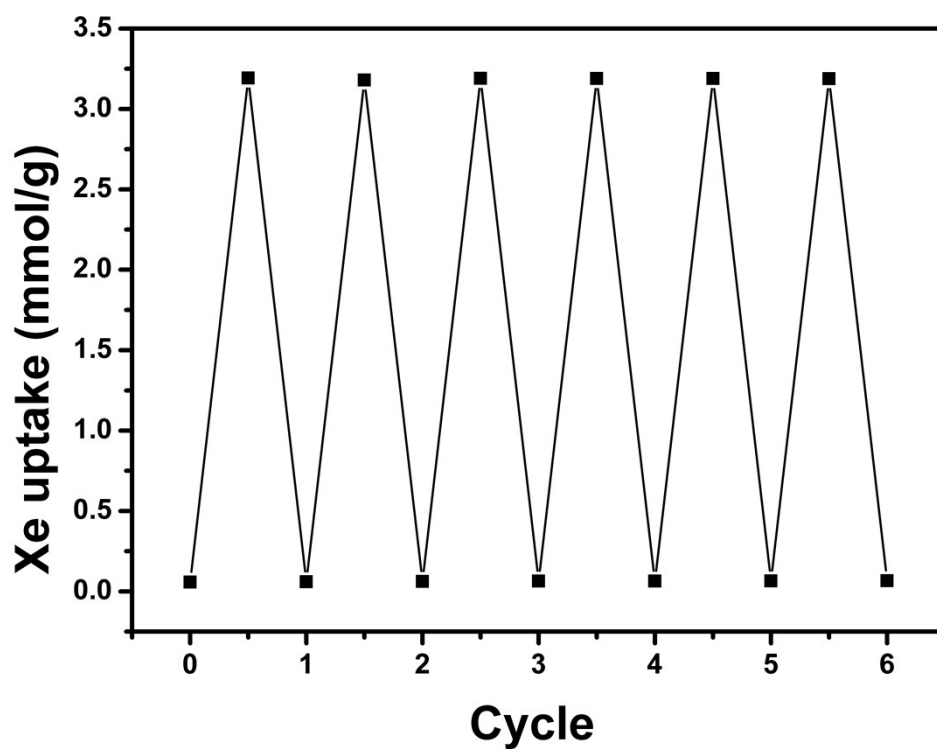


Figure S12. Xe adsorption/desorption cycling data on MOF-Cu-H at 298k and 1bar.

Calculation procedures of isotheric adsorption enthalpy

The isosteric enthalpy (Q_{st}) were calculated by the Clausius-Clapeyron equation :

$$\frac{Q_{st}}{R} = \frac{d(\ln P)}{d(1/T)} \quad (3)$$

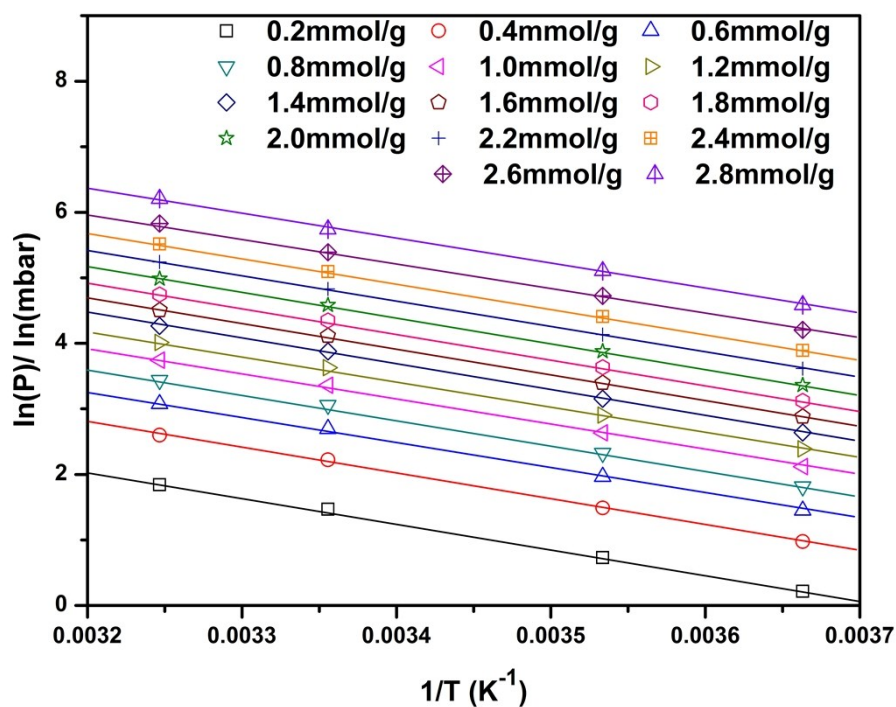


Figure S13. Van't Hoff isochore graphs for Xe adsorption on MOF-Cu-H for temperatures 273 K, 283 K, 298 K and 308 K, as a function of the amount adsorbed (n) ranging from 0.2-2.8 mmol/g.

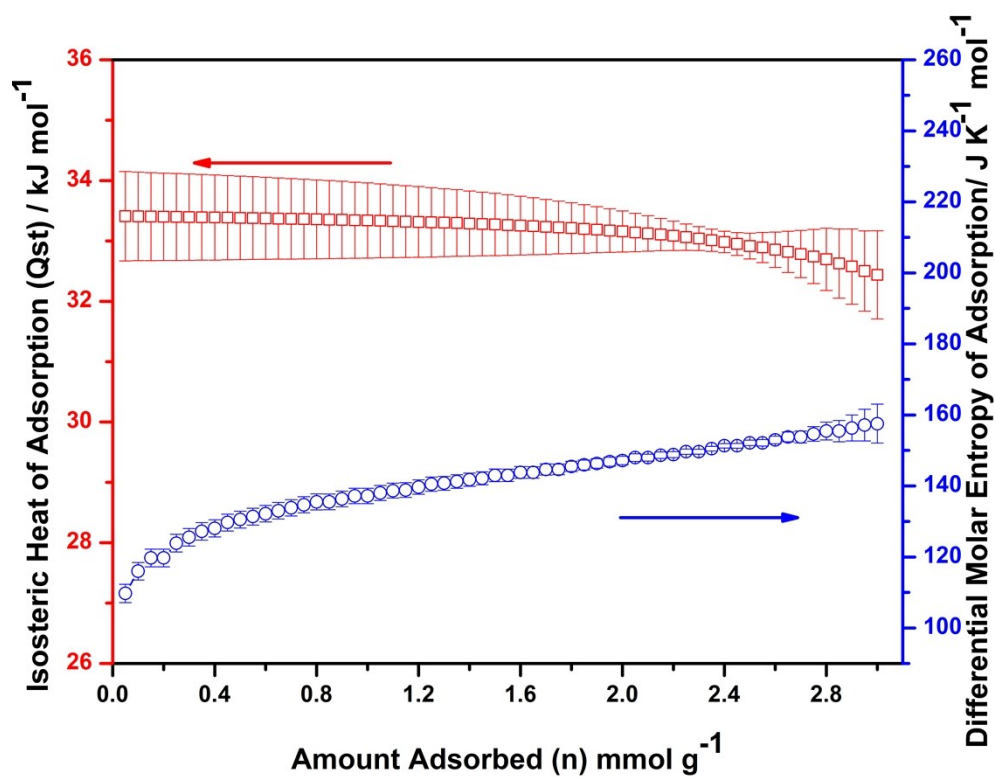


Figure S14. Isosteric heat ($Q_{st}/\text{kJ mol}^{-1}$) and differential molar heat ($\Delta S/\text{J K}^{-1}\text{ mol}^{-1}$) of adsorption on MOF-Cu-H for Xe as a function of the amount adsorbed (mmol g^{-1}) for the temperature range 273-308K.

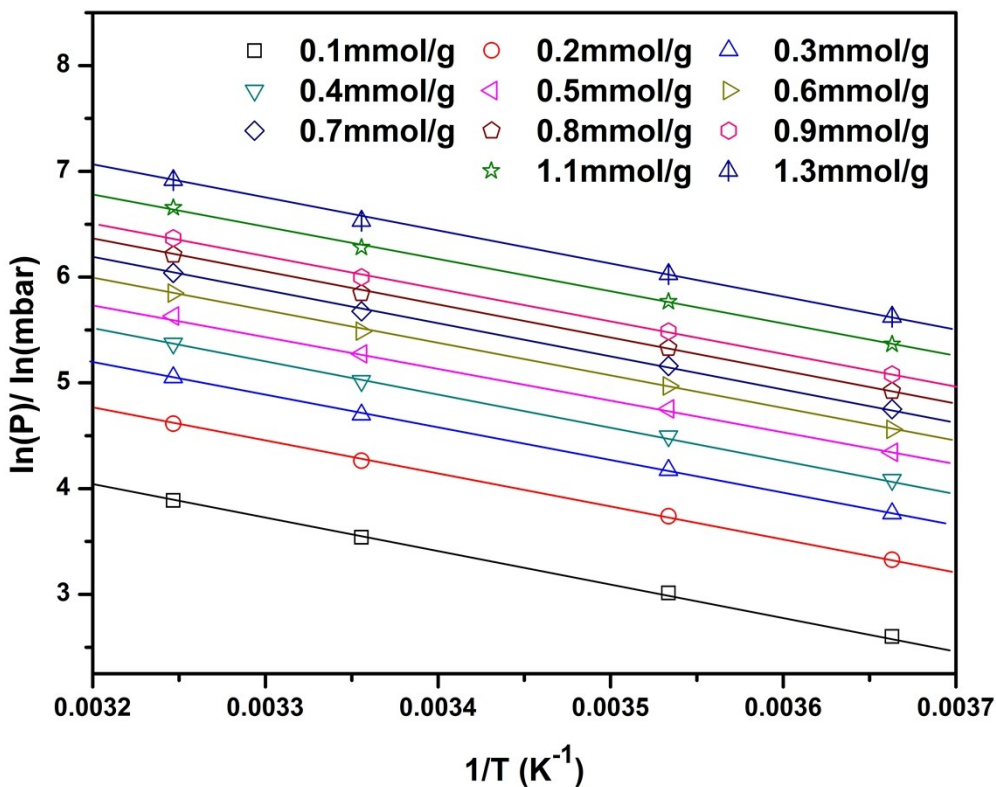


Figure S15. Van't Hoff isochore graphs for Kr adsorption on MOF-Cu-H for temperatures 273 K, 283 K, 298 K and 308 K, as a function of the amount adsorbed (n) ranging from 0.1-1.3 mmol/g.

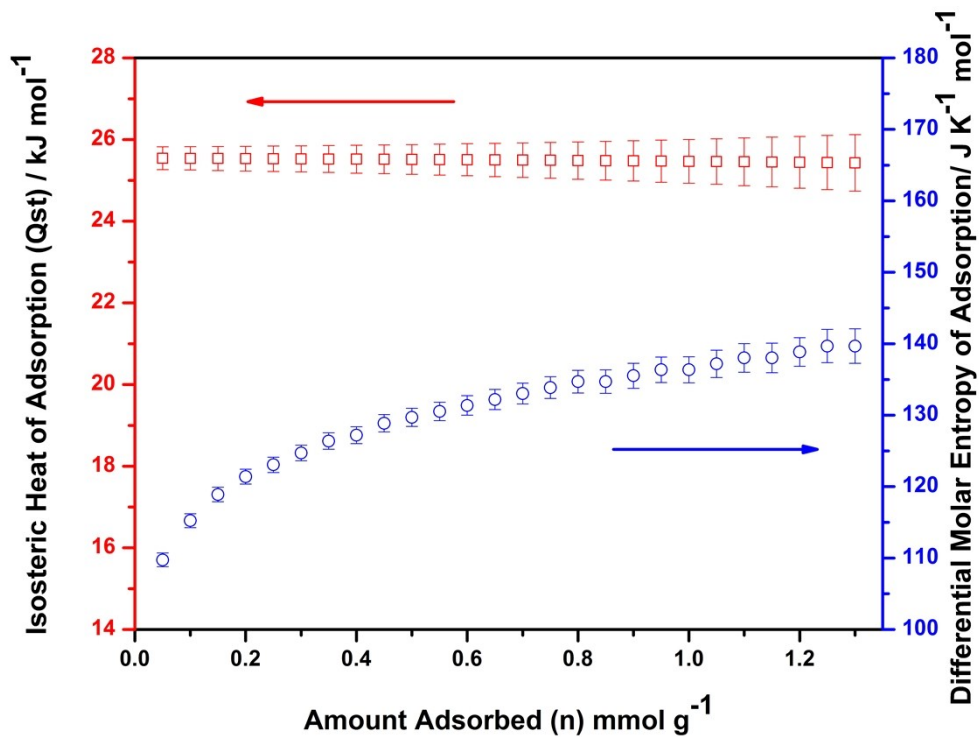


Figure S16. Isosteric heat ($Q_{st}/\text{kJ mol}^{-1}$) and differential molar heat ($S/\text{J K}^{-1} \text{mol}^{-1}$) of adsorption on MOF-Cu-H for Kr as a function of the amount adsorbed (mmol g^{-1}) for the temperature range 273-308K.

Henry's constant fitting

The low range of the adsorption isotherm is nearly linear which corresponds to Henry's law behavior. The Henry's constant of MOF-Cu-H were obtained from a linear fit to the in low pressure part of the isotherm. The Henry's constants of other reported porous materials were obtained from Thallapally's paper [D. Banerjee, C. M. Simon, A. M. Plonka, R. K. Motkuri, J. Liu, X. Chen, B. Smit, J. B. Parise, M. Haranczyk and P. K. Thallapally, Nat. Commun., 2016, 7, 11831.].

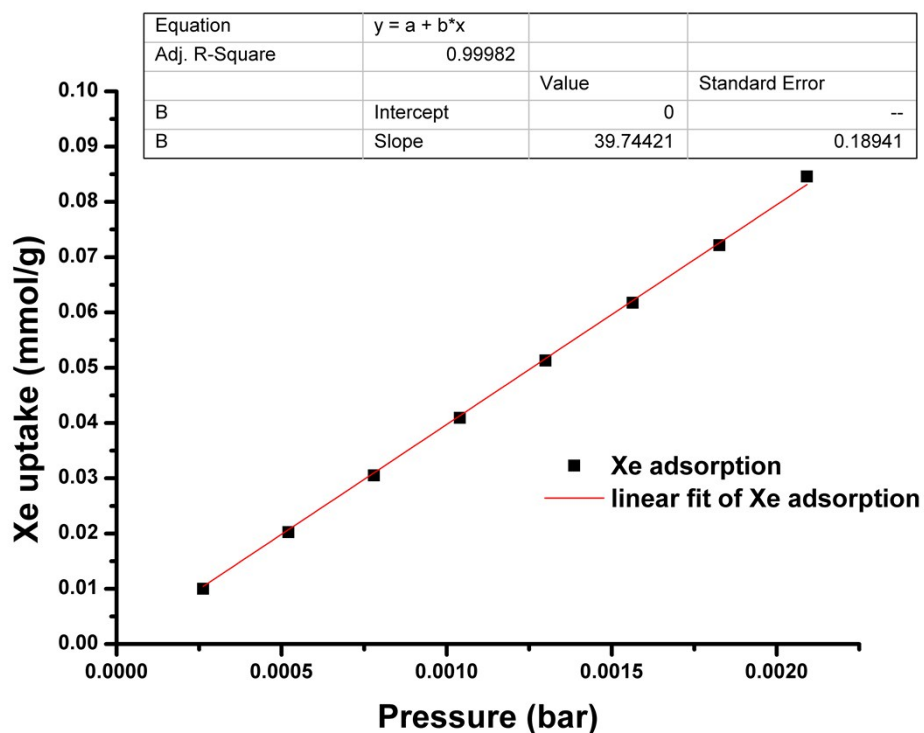


Figure S17. Henry coefficient fitting of Xe adsorption isotherm MOF-Cu-H at 298K.

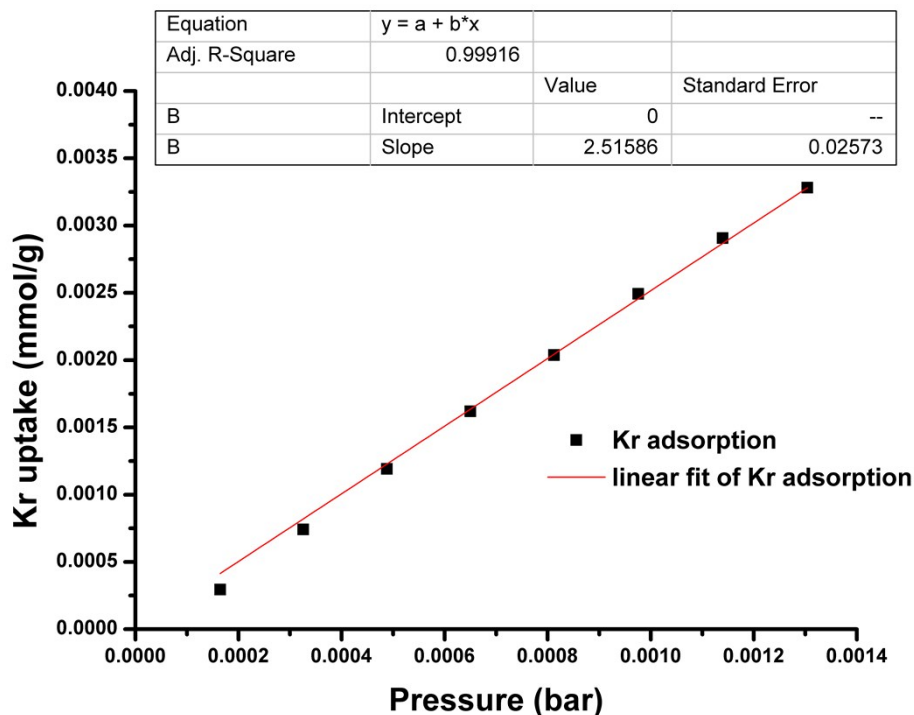


Figure S18. Henry coefficient fitting of Kr adsorption isotherm MOF-Cu-H at 298K.

Breakthrough experiments

In a typical breakthrough experiment, about 205 mg samples of MOF-Cu-H, were individually packed into three steel columns (the steel column was 20cm long in length with 4 mm of inner (0.64cm outer) diameter with silica wool filling the void space. The adsorbents were heated at 423 K under vacuum conditions for 10 hours and then activated by flowing a helium flow at 323 K for 2 hours before the temperature of the columns were decreased to 298 K. A circulator bath was used to maintain the temperature of the columns at 298 K. The flow of helium gas stream was turned off while the target gas mixtures were sent into the column. The flow of helium and targeted gas mixture was controlled by two Mass Flow Controllers with flow velocity of 5 ml/min. The downstream was monitored by a Hiden mass spectrometer (HPR 20). Adsorbed amounts of Xe and Kr were calculated by integrating the resulting breakthrough curves by considering dead volume times, which were measured by helium gas under the same flow rate.

The adsorption capacity was estimated from the breakthrough curves using the following equation:

$$n_{\text{adsi}} = FC_i t_i \quad (4)$$

Where n_{adsi} is the adsorption capacity of the gas i , F is the total molar flow, C_i is the concentration of the gas i entering the column and the t_i is the time corresponding to the gas i , which is estimated from the breakthrough profile.

The selectivity was then calculated according to the equation:

$$S_{A/B} = (X_A/X_B)/(Y_A/Y_B) \quad (5)$$

Where X_A and X_B are the mole fractions of the gases A and B in the adsorbed phase and Y_A and Y_B are the mole fractions of the gases A and B in the bulk phase.

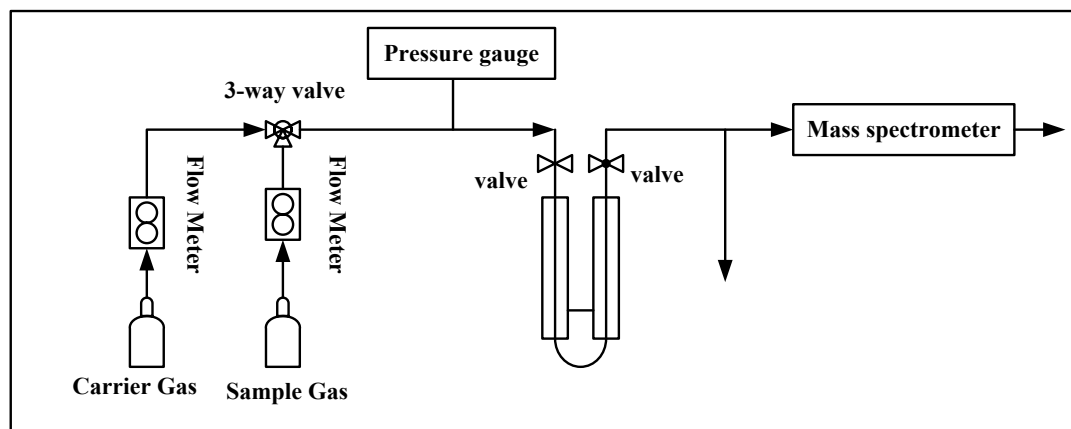


Figure S19. Representation of the dynamic breakthrough experiment.

Ideal Adsorbed Solution Theory:

The ideal adsorbed solution theory (IAST)^[1] was used to predict the equimolar binary mixture adsorption of CO₂ and CH₄ from the experiment pure-gas isotherm. The single-component isotherms were fit to a dual-site Langmuir-Freundlich equation:

$$q = q_{m1} \cdot \frac{b_1 \cdot P^{1/n_1}}{1 + b_1 \cdot P^{1/n_1}} + q_{m2} \cdot \frac{b_2 \cdot P^{1/n_2}}{1 + b_2 \cdot P^{1/n_2}} \quad (1)$$

Here, P is the pressure of the bulk gas at equilibrium with the adsorbed phase (kPa), q is the adsorbed amount per mass of adsorbent (mol/kg), q_{m1} and q_{m2} are the saturation capacities of sites 1 and 2 (mol/kg). b_1 and b_2 are affinity coefficient of sites 1 and 2

(1/kPa), and n_1 and n_2 represent the deviations from an ideal homogeneous surface.

Although this is not the only model that can be used to fit the data, IAST requires a precise fit of the experimental data to the model in order to accurately perform the necessary integrations.^[2-4]

Reference

- [1] Myers, A. L.; Prausnitz, J. M. *AIChE J.* 1965, **11**, 121.
[2] Babarao, R.; Hu, Z. Q.; Jiang J. W.; Chempath, S.; Sandler, S. I. *Langmuir*, 2007, **23**, 659.
[3] Goetz, V.; Pupier, O.; Guillot, A. *Adsorption*, 2006, **12**, 55.
[4] Bae, Y. S.; Mulfort K. L.; Frost, H.; Ryan, P.; Punnathanam, S.; Broadbelt, L. J.; Hupp, J. T.; Snurr, R. Q. *Langmuir*, 2008, **24**, 8592.

Dual Site Langmuir-Freundlich Model for Xe/Kr, and Xe/N₂ Adsorption

Isotherms

On the basis of the Dual site Langmuir-Freundlich (DSLFF) model: **(II)**

$$N = N_1^{\max} \times \frac{b_1 p^{1/n_1}}{1 + b_1 p^{1/n_1}} + N_2^{\max} \times \frac{b_2 p^{1/n_2}}{1 + b_2 p^{1/n_2}} \quad \text{(II)}$$

Where p (unit: Kpa) is the pressure of the bulk gas at equilibrium with the adsorbed phase, N (unit: mol/Kg) is the adsorbed amount per mass of adsorbent, N_1^{\max} and N_2^{\max} (unit: mol/Kg) are the saturation capacities of sites 1 and 2, b_1 and b_2 (unit: 1/kPa) are the affinity coefficients of sites 1 and 2, and n_1 and n_2 represent the deviations from an ideal homogeneous surface. Here, the single-component CO₂, CH₄, and N₂ adsorption isotherms have been fit to enable the application of IAST in simulating the performance of MOF-Cu-H, under a mixed component gas. The fitting parameters of DSLFF equation are listed in Table S5. Adsorption isotherms and gas selectivities calculated by IAST for mixed Xe/Kr (Xe/Kr = 20:80), Xe/N₂ (Xe/N₂ =

1:99) in the MOF-Cu-H.

Table S1. Equation parameters for the DSLF isotherm model for the single-component isotherms of Xe, Kr and N₂ in MOF-Cu-H at 298K.

adsorbent	Adsorbates	N_1^{\max} (mmol/g)	b_1 (kPa ⁻¹)	n_1	N_2^{\max} (mmol/g)	b_2 (kPa ⁻¹)	n_2
MOF-Cu-H	Xe	0.525	0.0426	0.522	2.85	0.144	0.989
	Kr	3.44	0.00613	0.960	0.127	0.0142	0.631
	N ₂	1.59	0.0013	1.063	12.4	0.00018	1.046

First-principles calculations

The grand canonical Monte Carlo (GCMC) method was used as implemented in the RASPA 2.0 code^[5] to obtain initial adsorption of Xe or Kr atoms in the MOF-Cu-H. The MOF framework was treated as rigid. A 3x3x3 supercell was adopted in the simulation. 2×10^6 steps were used as equilibration stage, and 6×10^6 more steps were performed to get the averaged atom adsorption sites. The Lennard-Jones potential parameters for Xe, Kr, and the MOF atoms from the generic MOF force field in RASPA were adopted, which were similar with the values collected in Ref.[6], which were taken from the Dreiding force field and the UFF.^[7, 8] The parameters for Xe and Kr were $\epsilon/kb = 221.0$ and $166.4K$, and $\sigma = 4.1$ and 3.636 \AA , respectively. The Lorentz-Berthelot mixing rules were adopted for the LJ cross interactions. The temperature of 298K and pressure of 10^5 Pa was applied for the pure Xe and Kr adsorption. It could be found that there were four cavities in the unit cell of MOF-Cu-H for Xe or Kr adsorption, and there was at most one atom occupying each cavity at the same time. The Xe and Kr atoms adsorbed at the similar sites but with different absorption amounts, which was about 3.82Xe and 2.53Kr, respectively.

The obtained structures with averaged inerted gas atom positions were further relaxed using first-principles density functional theory (DFT) calculations. The VASP code was used.^[9, 10] The Perdew-Bruke-Ernzerhof (PBE)^[11] version of generalized-gradient approximation (GGA) of density functional was used with the Grimme D2 method to account for the van der Waals interactions.^[12] The electron-ion interactions were described by the projector-augmented wave (PAW) method. The energy cutoff for plane-wave basis-set expansion was 450eV, and the Γ k-point was used for k-space sampling. The convergence criteria for total and residual forces were

set to 10^{-5} eV per cell and 0.02 eV/Å for each ion. First, the experimental structure of the unit cell of MOF was relaxed without lattice variation, then the inert gas atoms were added one by one. The binding energies of Xe or Kr in MOF were calculated following:

$$E_{\text{bind}} = (E_{\text{tot}}(\text{MOF}-n \text{ gas}) - E_{\text{tot}}(\text{MOF}) - n E_{\text{tot}}(\text{gas})) / n \quad (1),$$

Where n was the number of adsorbed Xe or Kr atoms, $E_{\text{tot}}(\text{MOF}-n \text{ gas})$, $E_{\text{tot}}(\text{MOF})$, $E_{\text{tot}}(\text{gas})$ were the total energies of the MOF adsorbed n Xe or Kr atoms, the clean MOF, and the isolated Xe or Kr atoms, respectively. The E_{bind} was thus the averaged binding energy per Xe or Kr atom of this MOF. The E_{bind} values were the same for different number of adsorbed atoms, from one to four in a MOF unit cell. The calculated values were presented in Table S2. The binding energy of Xe was stronger than Kr, which is consistent with larger amount of Xe than Kr in GCMC simulations. The adsorption site of Xe or Kr is located in the small cage of MOF-Cu-H that contains five organic linkers and three dicopper paddle-wheel SBUs. The geometry structure of four Xe adsorbed in MOF-Cu-H were shown in Fig.S17 and Fig S18. We also tested the adsorption site of Xe in the center of 1D channel, after geometry relaxation, the calculated E_{bind} is -0.28 eV, which is about 0.12 eV higher than the one inside the small cage presented in Table S2. This result indicates that the site inside the small cages would be much more favorable than in the 1D channel thermodynamically. It is consistent with the above GCMC results at the mild condition that only the Xe in the small cages are found.

Table S2. The binding energy of Xe and Kr in MOF with different number of atoms per unit cell.

Number of inert gas atoms in the MOF unit cell	E_{bind} of Xe (eV/Xe)	E_{bind} of Kr (eV/Kr)
1	-0.40	-0.27
2	-0.40	-0.27
3	-0.40	-0.27
4	-0.40	-0.27

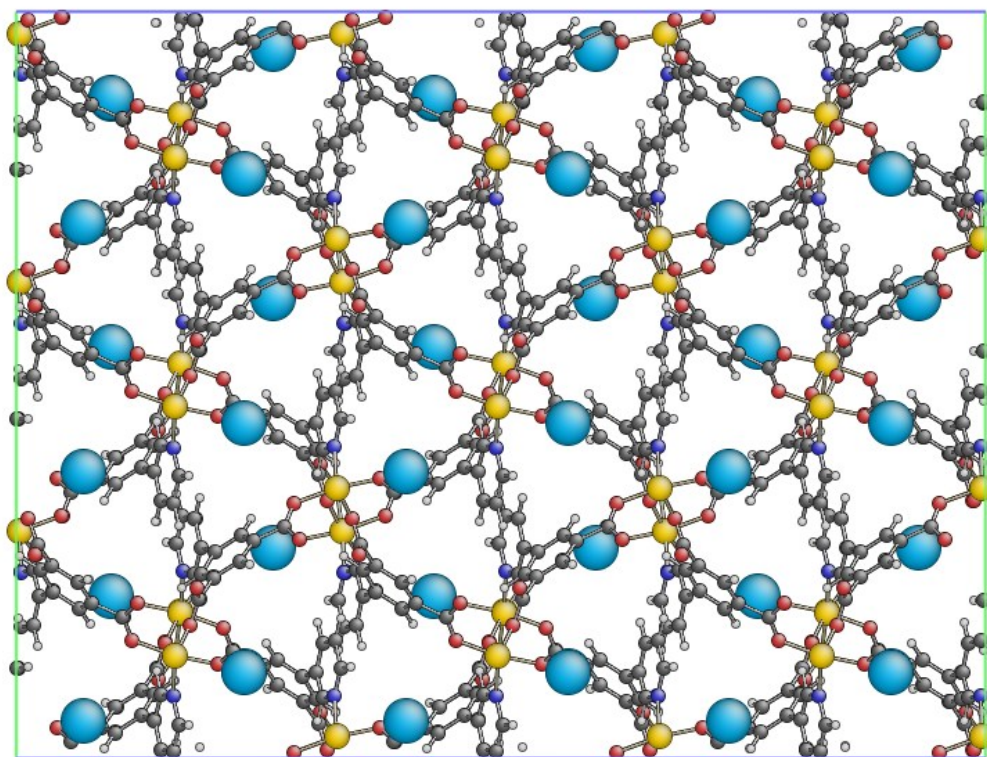


Figure 20. The adsorbed Xe in MOF-Cu-H. The blue, yellow, red, gray, and white circles represent the Xe/Kr, Cu, O, C, and H atoms, respectively.

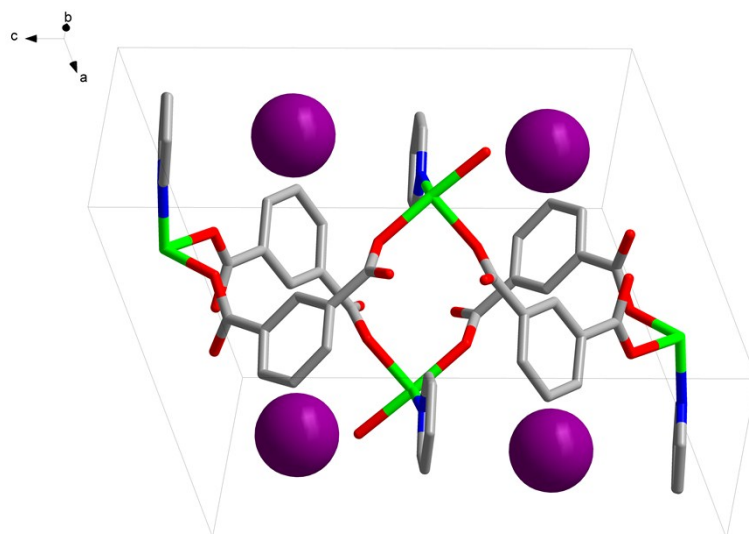


Figure S21. Four Xe atoms adsorbed in one crystal unit cell of MOF-Cu-H. The purple, green, red

and gray balls represent the Xe/Kr, Cu, O, C, and H atoms, respectively.

Reference

- [5]. Dubbeldam, D., et al., RASPA: molecular simulation software for adsorption and diffusion in flexible nanoporous materials. *Molecular Simulation*, 2016. 42(2): p. 81-101.
- [6]. Wang, Q., et al., Adsorption and Separation of Xe in Metal – Organic Frameworks and Covalent – Organic Materials. *The Journal of Physical Chemistry C*, 2014. 118(19): p. 10221-10229.
- [7]. Mayo, S.L., B.D. Olafson and W.A. Goddard, DREIDING: a generic force field for molecular simulations. *The Journal of Physical Chemistry*, 1990. 94(26): p. 8897-8909.
- [8]. Kresse, G. and J. Furthmüller, Efficiency of ab-initio total energy calculations for metals and semiconductors using a plane-wave basis set. *Computational Materials Science*, 1996. 6(1): p. 15-50.
- [9]. Furthmüller, J. and G. Kresse, Efficient iterative schemes for ab initio total-energy calculations using a plane-wave basis set. *Physical Review B*, 1996. 54(16): p. 11169-11186.
- [10]. Burke, K., M. Ernzerhof and J.P. Perdew, Generalized Gradient Approximation Made Simple. *Physical Review Letters*, 1996. 77(18): p. 3865-3868.
- [11]. Grimme, S., Semiempirical GGA-type density functional constructed with a long-range dispersion correction. *Journal of Computational Chemistry*, 2006. 27(15): p. 1787-1799.
- [12]. Blöchl, P.E., Projector augmented-wave method. *Physical Review B*, 1994. 50(24): p. 17953-17979.

Table S3. Xenon adsorption capacity and Xe/Kr selectivity at room temperature from gas mixtures at dilute condition

Sorbent	Xe uptake (mmol/kg)	Xe/Kr Selectivity derived from Henry coefficients	Concentration of Xe and Kr
MOF-Cu-H	13.0	15.8	350 p.p.m Xe, 35 p.p.m Kr
SBMOF-1	13.2	16.2	400 p.p.m Xe, 40 p.p.m Kr
CC3	11.0	12.8	400 p.p.m Xe, 40 p.p.m Kr
Ni-MOF-74	4.8	5.8	400 p.p.m Xe, 40 p.p.m Kr

Table S4. Xe uptakes and separation in selected porous materials.

Novel porous materials	Specific surface area (m ² /g)	The capacity of Xe (mmol/g)	Xe/Kr selectivity	Xe Qst (kJ/mol)	Ref
MOF-Cu-H	868	3.19 ¹	15.8 ^a /16.7 ^b	33.41 ± 0.74	This work
IRMOF-1	3400	1.98 ¹	3 ^b	15	[13]
Monohalogenated IRMOF-2 series	1900-3100	1.5-2.0 ²	--	11-15	[14]
Al-MIL-53	1300	2.0 ⁵	--	--	[15]
CC3	624	2.32 ¹	12.8 ^a	31.3	[16]
NiMOF-74	950	4.16 ¹	7.3 ^a /5-6 ^b	22	[17,18,19]
Ag@NiMOF-74	749.7	4.82 ¹	6.8 ^b	23.6	[19]
Noria	40	1.55 ¹	9.4 ^b	24.5-26.9	[20]
Co ₃ (HCOO) ₆	300	2 ⁴	12 ^b	28	[21]
HKUST-1	1710	3.18 ¹	2.6 ^c	26.9	[22]
MFU-4L	3500		4.7(310 K) ^a	20	[23]
SBMOF-2	195	2.83 ¹	10 ^b	26.4	[24]
SBMOF-1	145	1.38 ¹	16 ^a		[25]
MOF-505	1030	2.2 ⁴	9-10 ^c		[22]
FMOFCu	58	~0.45 ¹	1 ^b	10(>0°C)	[26]

UTSA-49	710.5	3.0 ¹	9.2 ^b	23.53 ± 0.54	[27]
CROFOUR-1-Ni	505 ^L	1.8 ¹	22 ^{b/} 19.8 ^c	37.4	[28]
CROFOUR-2-Ni	475 ^L	1.6 ¹	15.5 ^{b/} 14.3 ^c	30.5	[28]
Co-MOF-74	1346	6.71 ³	10.5 ^{b/} 6.4 ^c	28.4	[29]
Mg-MOF-74	1486	~6.5 ⁶	7 ^a	23.5	[29]
Zn-MOF-74	844	~4.5 ⁶	7 ^a	23.8	[29]
UiO-66(Zr)	1199	1.58	7.15 ^a	25	[30]
MIL-101(Cr)	3445	1.38	5.33 ^a	21.4	[30]
MIL-100(Fe)	1947	1.14	5.59 ^a	20.9	[30]

- a. calculated from Henry coefficients at 298K b. predicted using IAST c. calculated from breakthrough experiments (298 K 20/80 Xe/Kr mixture) L. the surface area calculated by Langmuir method, all the other surface areas are calculated by BET method. 1. 298K, 1bar 2. 292K, 1bar 3. 293K, 1bar 4. 298K, 0.2bar 5. 308K, 1bar 6. 283K, 1bar

Reference

- [13] U. Mueller, M. Schubert, F. Teich, H. Puetter, K. Schierle-Arndt and J. Pastre, *Journal of Materials Chemistry*, 2006, **16**, 626-636.
- [14] S. T. Meek, S. L. Teich-McGoldrick, J. J. Perry, J. A. Greathouse and M. D. Allendorf, *The Journal of Physical Chemistry C*, 2012, **116**, 19765-19772.
- [15] A. Boutin, M. A. Springuel-Huet, A. Nossov, A. Gédéon, T. Loiseau, C. Volkringer, G. Férey, F. X. Coudert and A. H. Fuchs, *Angewandte Chemie International Edition*, 2009, **48**, 8314.
- [16] L. Chen, P. S. Reiss, S. Y. Chong, D. Holden, K. E. Jelfs, T. Hasell, M. A. Little, A. Kewley, M. E. Briggs, A. Stephenson, K. M. Thomas, J. A. Armstrong, J. Bell, J. Busto, R. Noel, J. Liu, D. M. Strachan, P. K. Thallapally and A. I. Cooper, *Nature materials*, 2014, **13**, 954.
- [17] P. K. Thallapally, J. W. Grate and R. K. Motkuri, *Chemical Communications*, 2012, **48**, 347.
- [18] J. Liu, P. K. Thallapally and D. M. Strachan, *Langmuir*, 2012, **28**, 11584.
- [19] J. Liu, D. M. Strachan and P. K. Thallapally, *Chemical Communications*, 2014, **50**, 466.
- [20] R. S. Patil, D. Banerjee, C. M. Simon, J. L. Atwood and P. K. Thallapally, *Chemistry-A European Journal*, 2016, **22**, 12618.
- [21] H. Wang, K. Yao, Z. Zhang, J. Jagiello, Q. Gong, Y. Han and J. Li, *Chemical Science*, 2014, **5**, 620.
- [22] Y.-S. Bae, B. G. Hauser, Y. J. Colón, J. T. Hupp, O. K. Farha and R. Q. Snurr, *Microporous and Mesoporous Materials*, 2013, **169**, 176.
- [23] A. S. Dorcheh, D. Denysenko, D. Volkmer, W. Donner and M. Hirscher, *Microporous and Mesoporous Materials*, 2012, **162**, 64.
- [24] X. Chen, A. M. Plonka, D. Banerjee, R. Krishna, H. T. Schaefer, S. Ghose, P. K. Thallapally,

- and J. B. Parise, *Journal of the American Chemical Society*, 2015, **137**, 7007.
- [25] D. Banerjee, C. M. Simon, A. M. Plonka, R. K. Motkuri, J. Liu, X. Chen, B. Smit, J. B. Parise, M. Haranczyk and P. K. Thallapally, *Nature communications*, 2016, **7**, 11831.
- [26] C. A. Fernandez, J. Liu, P. K. Thallapally and D. M. Strachan, *Journal of the American Chemical Society*, 2012, **134**, 9046.
- [27] S. Xiong, Q. Liu, Q. Wang, W. Li, Y. Tang, X. Wang, S. Hu and B. Chen, *Journal of Materials Chemistry A*, 2015, **3**, 10747.
- [28] M. H. Mohamed, S. K. Elsaidi, T. Pham, K. A. Forrest, H. T. Schaefer, A. Hogan, L. Wojtas, W. Xu, B. Space, M. J. Zaworotko and P. K. Thallapally, *Angewandte Chemie International Edition*, 2016, **55**, 8285.
- [29] S.-J. Lee, K. C. Kim, T.-U. Yoon, M.-B. Kim, Y.-S. Bae, *Microporous and Mesoporous Materials*, 2016, **236**, 284-291.
- [30] S.-J. Lee, T.-U. Yoon, A.-R. Kim, S.-Y. Kim, K.-H. Cho, Y. K. Hwang, J.-W. Yeon, Y.-S. Bae, *Journal of Hazardous Materials*, 2016, **320**, 513-520.